ISSN 1674-1056
http://cpb.iphy.ac.cn
http://iopscience.iop.org/cpb
中国物理 B
Chinese Physics
中国物理
Chinese Physics B

Estimation of tungsten production from the upper divertor in EAST during edge localized modes

Jing Ou(欧靖)[1,2], Nong Xiang(项农)[1,2], Zong-Zheng Men(门宗政)[1], Ling Zhang(张凌)[1], Ji-Chan Xu(许吉禅)[1], Wei Gao(高伟)[1]

Citation: Chin. Phys. B . 2019, 28(12): 125201 . **doi:** 10.1088/1674-1056/ab5279
Journal homepage: http://cpb.iphy.ac.cn; http://iopscience.iop.org/cpb

What follows is a list of articles you may be interested in

Dust charging and levitating in a sheath of plasma containing energetic particles

Jing Ou(欧靖), Xiao-Yun Zhao(赵晓云), Bin-Bin Lin(林滨滨)
Chin. Phys. B . 2018, 27(2): 025204 . **doi:** 10.1088/1674-1056/27/2/025204

Sheath structure in plasma with two species of positive ions and secondary electrons

Xiao-Yun Zhao(赵晓云), Nong Xiang(项农), Jing Ou(欧靖), De-Hui Li(李德徽), Bin-Bin Lin(林滨滨)
Chin. Phys. B . 2016, 25(2): 025202 . **doi:** 10.1088/1674-1056/25/2/025202

A two-dimensional model of He/O_2 atmospheric pressure plasma needle discharge

Qian Mu-Yang, Yang Cong-Ying, Chen Xiao-Chang, Liu San-Qiu, Yan Wen, Liu Fu-Cheng, Wang De-Zhen
Chin. Phys. B . 2015, 24(12): 125203 . **doi:** 10.1088/1674-1056/24/12/125203

Effects of some parameters on the divertor plasma sheath characteristics and fuel retention in castellated tungsten tile gaps

Sang Chao-Feng, Dai Shu-Yu, Sun Ji-Zhong, Bonnin Xavier, Xu Qian, Ding Fang, Wang De-Zhen
Chin. Phys. B . 2014, 23(11): 115201 . **doi:** 10.1088/1674-1056/23/11/115201

Characteristics of wall sheath and secondary electron emission under different electron temperatures in a Hall thruster

Duan Ping, Qin Hai-Juan, Zhou Xin-Wei, Cao An-Ning, Chen Long, Gao Hong
Chin. Phys. B . 2014, 23(7): 075203 . **doi:** 10.1088/1674-1056/23/7/075203

Estimation of tungsten production from the upper divertor in EAST during edge localized modes*

Jing Ou(欧靖)[1,2,†], Nong Xiang(项农)[1,2], Zong-Zheng Men(门宗政)[1], Ling Zhang(张凌)[1], Ji-Chan Xu(许吉禅)[1], and Wei Gao(高伟)[1]

[1] *Institute of Plasma Physics, Chinese Academy of Sciences, Hefei* 230031, *China*
[2] *Magnetic Fusion Theory, Chinese Academy of Sciences, Hefei* 230031, *China*

(Received 18 July 2019; revised manuscript received 22 October 2019; published online 29 November 2019)

During edge localized modes (ELMs), the sheath evolution in front of the Experimental Advanced Superconducting Tokamak (EAST) upper divertor is studied to estimate the sputtered tungsten (W) atoms from the divertor target. A large potential drop across the sheath is formed during ELMs by compared with inter-ELMs, and the maximum of sheath potential drop can exceed one thousand of eV in current EAST operation. Due to the enhancement of the sheath potential drop during ELMs, the W physical sputtering yield from the deuterium (D) ions and the impurity ions on the upper divertor target is found to be significant. It is established that the sputtered W yield during ELMs is at least higher by an order of magnitude than inter-ELMs, and D ions and carbon (C) ions are the main ions governing the W production for the current H-mode with ELMs discharges. With increase in the pedestal electron temperature, the maximum of the D and C ion impact energy during ELMs shows a nearly linear increase, and the D ions have sufficient impact energy to cause the strong W physical sputtering. As a consequence, the D ions may dominate the sputtered W flux from the divertor target when the C concentration is controlled less than one percent for the higher heating power H-mode with ELM discharges in near future.

Keywords: sheath, edge localized modes, impact energy

PACS: 52.40.Kh, 52.25.Vy, 52.40.Hf **DOI:** 10.1088/1674-1056/ab5279

1. Introduction

The edge localized modes (ELMs) driven by the quasi-periodic magnetohydrodynamic instabilities are often observed in tokamak plasmas with the high-confinement mode (H-mode). ELMs will cause the transient energy loss of the plasma stored energy and expel the impurities from the main-edge plasma region before they penetrate the core plasma. Most of the particle and energy fluxes induced by ELM bursts are transported to the divertor regions and then lead to the excessive heat load on the divertor plate and strong ion impact energy on the divertor material. As a consequence, the impurity releases from the divertor plate and the resultant lifetime of the material decreases. Furthermore, the impurity from the divertor target can migrate into the core plasma to deteriorate the plasma confinement. Hence, the ELM event and a series of problems induced by ELMs may limit the H-mode operation regime. With low sputtering yield and high melting point, tungsten (W) material has been used as the divertor target material in several tokamaks,[1–3] and it is also suggested as the divertor target material instead of carbon (C) in next fusion devices such as ITER and CFETR.[4] In the Experimental Advanced Superconducting Tokamak (EAST), the upper graphite divertor was upgraded into a full W one with ITER-like actively water-cooled monoblock structure in 2014.[3] With upper W divertor, the EAST obtained over 60 s in fully noninductive H-mode plasma operation in 2016.[5] However, under some conditions, the W from the upper divertor can degrade the plasma confinement and even cause the termination of the plasma discharge.[6] Since the core plasma has a very low tolerability to the W concentration,[7] the control of W production and W radiation are the key issues for long-pulse high performance operation in the EAST.

The physical sputtering is the main process of W production. In this process, the sheath plays a crucial role in determining the W physical sputtering since it can change the ion bombardment energy on the W material. For a collisionless sheath, the ion impact energy on the material is determined by the ion energy at the sheath edge and the ion acceleration across the sheath. In L-mode or inter-ELM H-mode deuterium (D) plasma operation, the potential drop across the sheath Φ approximates to $-e_0\Phi \approx 3k_{\rm B}T_{\rm e,0}$ with the elementary charge e_0, the Boltzmann's constant $k_{\rm B}$ and electron temperature near the divertor $T_{\rm e,0}$. During the ELMs, Φ depends on the pedestal electron temperature.[8–10] Based on the sheath evolution obtained from the analytical model during ELMs, it is shown in the JET that the D ion is the main trigger of the W source while the contribution of the beryllium ion is lower by an order of magnitude because of the small concentration.[11] In

*Project supported by the National Key R&D Program of China (Grant Nos. 2017YFE0300400 and 2017YFE0301300), the National Natural Science Foundation of China (Grant Nos. 11475223 and 11775257), the National Magnetic Confinement Fusion Science Program of China (Grant No. 2015GB101003), and also partly supported by AHNSF of China (Grant No. 1808085J07).

†Corresponding author. E-mail: ouj@ipp.ac.cn

© 2019 Chinese Physical Society and IOP Publishing Ltd

the current EAST, H-mode discharges with upper W divertor configuration have been operated with the mixed wall materials and lithium (Li) coating.[5] The W production caused by multiple impurity ions must be estimated. For the L-mode discharges, it was found that the W erosion is governed mainly by C ion bombardment instead of molybdenum (Mo) from the first wall material.[12,13] For the H-mode with ELMs discharges, the W erosion and transport during the ELMs have been investigated.[14,15] However, effect of the multiple impurity ions on the W production with the sheath evolution during ELMs is not taken into account.

In this work, we perform the evolution of sheath potential in front of the upper divertor in the EAST during an ELM pulse, and then discuss the following questions: What is the main element to determine the sheath potential? How much is the sputtered W yield by the multiple ion bombardment in current discharges? How do the contribution of the D ions and C ions to the W source vary with the input power? All these questions are related to the impurity control and plasma confinement. The rest of this paper is organized as follows: The models for the ELM and the sheath are described in Section 2. Section 3 shows the multiple ion impact energies on the W material and the corresponding W production during ELMs. Finally, a summary is shown in Section 4.

2. Model description

The ELMs transport in scrape-off-layer (SOL) can be described by the analytical model,[8,16] the Vlasov model,[16,17] particle-in-cell (PIC)[9,10] and fluid models. The 'free-streaming' kinetic model (FSM) describes ELMs as a quasi-neutral plasma bunch expanding along the magnetic field lines into the SOL without collisions.[8] It is shown that the results of the particles and energy fluxes on the divertor target obtained by the FSM agree well with the collisionless Vlasov model[17] and the ion impact energy of the peak power density at the strike point predicted by the FSM matches the JET experimental result.[11]

In the FSM, the parallel temperature is constant in space and given by[8]

$$T_{\alpha,\mathrm{ELM}}(t) = \frac{T_\alpha^{\mathrm{ped}}}{1+(tC_\mathrm{s}^{\mathrm{ped}}/\sigma_0)^2}, \tag{1}$$

and the density is

$$n_{\alpha,\mathrm{ELM}}(t) = \frac{n_\alpha^{\mathrm{ped}}}{\sqrt{1+(tC_\mathrm{s}^{\mathrm{ped}}/\sigma_0)^2}} \exp\left[-\frac{L_\parallel^2}{2\sigma_0^2(1+(tC_\mathrm{s}^{\mathrm{ped}}/\sigma_0)^2)}\right], \tag{2}$$

where the label α denotes the ion, electron, or impurity, respectively. The parallel connection length $L_\parallel$ is defined as the typical distance between the outer midplane and the outer divertor target. $C_\mathrm{s}^{\mathrm{ped}} = \sqrt{k_\mathrm{B}(T_\mathrm{i}^{\mathrm{ped}}+T_\mathrm{e}^{\mathrm{ped}})/m_\mathrm{i}}$ is sound velocity with pedestal temperature T_α^{ped} and the ion mass m_i; σ_0 is the parallel extent of the source, and $\sigma_0 = 0.1L_\parallel$ is used.[17] Here the effect of the impurities on the FSM is not taken into account since impurity concentration is less than a few percent in the EAST, and then plasma density at the pedestal region $n_\mathrm{e}^{\mathrm{ped}} \approx n_\mathrm{i}^{\mathrm{ped}} = n_{\mathrm{ped}}$ and $T_\alpha^{\mathrm{ped}} = T_{\mathrm{ped}}$ are assumed in the following discussion.

In the EAST, the timescale of the ELM usually is $\omega_{\mathrm{ELM}} \approx 10^5$–$10^7$ s^{-1}. Near the divertor region, the typical plasma density at sheath edge during inter-ELMs, i.e., background density, $n_{\mathrm{e},0}^0 = 10^{19}$ m^{-3}, the electron frequency is $\omega_{\mathrm{pe}} = \sqrt{n_{\mathrm{e},0}^0 e_0^2/(\varepsilon_0 m_\mathrm{e})} \approx 10^{11}$ s^{-1}, and the D ion frequency is $\omega_{\mathrm{pi}} = \sqrt{n_{\mathrm{e},0}^0 e_0^2/(\varepsilon_0 m_\mathrm{i})} \approx 2.8\times10^9$ s^{-1}, where ε_0 is permittivity of free space. Because the timescale of the ELM is much smaller than the electron and ion frequencies, here a steady-state collisionless sheath model is introduced. Moreover, we assume that the impurity density is much lower than the main ion and thus the impurity does not disturb the plasma sheath.[18] At the sheath edge, the one-dimensional electron distribution function is assumed as

$$f_{\mathrm{e},j}(v) = \frac{I_{\mathrm{e},j} n_{\mathrm{e},j}^0}{\sqrt{2\pi}v_{\mathrm{te},j}} \exp\left(-\frac{(v-\bar{v}_{\mathrm{e},j})^2}{2v_{\mathrm{te},j}^2}\right), \quad \text{for } v_{\mathrm{ce}} < v, \tag{3}$$

where the label $j = 0$ and ELM denoting the background electron and the electron carried by ELMs (hot electrons), respectively; $n_{\mathrm{e},j}^0$ represents the density at sheath edge, the electron drifting velocity $\bar{v}_{\mathrm{e},j}$ represents the amount of the velocity shift of the electron distribution. Specifically, we assume that $\bar{v}_{\mathrm{e},0} = 0$ for the electrons; $v_{\mathrm{te},j} = \sqrt{T_{\mathrm{e},j}/m_\mathrm{e}}$ is the thermal velocity. The electron cut-off velocity is determined by the wall potential Φ as $v_{\mathrm{ce}} = -\sqrt{-2e_0\Phi/m_\mathrm{e}}$. This cut-off velocity yields the electron normalization coefficient $I_\mathrm{e} = 2/[1+\mathrm{erf}(\sqrt{-e_0\Phi/k_\mathrm{B}T_{\mathrm{e},j}})]$. Then, the electron fluxes to the target surface can be expressed as

$$\Gamma_{\mathrm{e},j} = \frac{I_{\mathrm{e},j} n_{\mathrm{e},j}^0 v_{\mathrm{te},j}}{\sqrt{2\pi}} \exp\left[\frac{e_0\Phi}{k_\mathrm{B}T_{\mathrm{e},j}}\right]. \tag{4}$$

The ion particle flux is a constant in a collisionless sheath

$$\Gamma_{\mathrm{i},j} = n_{\mathrm{i},j}^0 v_{i0,j}, \tag{5}$$

where $v_{\mathrm{i}0,j}$ is the ion velocity at the sheath edge. For the multi-ion-component plasma collisionless sheath, it is suggested from both analytical and numerical results that each ion species at the sheath edge should satisfy its own Bohm criterion,[19,20] i.e., $v_{\mathrm{i}0,j} = C_{\mathrm{s},j}$. For a sheath of more than one population of negatively charged particles, by following Riemann,[21] the Bohm velocity can be written as $C_{\mathrm{s},j} = \sqrt{(T_{\mathrm{i},j}+Z_{\mathrm{i},j}T_{\mathrm{e,eff}})/m_\mathrm{i}}$ with the ions charge states $Z_{\mathrm{i},j}$ and the effective electron temperature $T_{\mathrm{e,eff}}$ defined as $\frac{n^0}{k_\mathrm{B}T_{\mathrm{e,eff}}} = \frac{n_{\mathrm{e},0}^0}{k_\mathrm{B}T_{\mathrm{e},0}} + \frac{n_{\mathrm{ELM}}^0}{k_\mathrm{B}T_{\mathrm{ELM}}}$. Here, for the background ions, $T_{\mathrm{i},0} = T_{\mathrm{e},0}$ is assumed.

The Φ is obtained based on the zero current to the target surface,

$$\Gamma_{i,j} = \Gamma_{e,j}. \tag{6}$$

For the ions from the bulk plasma across the sheath, the average bombardment energy on the material is given by

$$E_{i,j} = 2k_B T_{i,j} + \frac{1}{2} m_{i,j} v_{i0,j}^2 - Z_{i,j} e_0 \Phi. \tag{7}$$

For the impurity ions, the bombardment energy depends on the $Z_{i,j}$. Usually, $Z_{i,j}$ is determined by the electron density and electron temperature,[22] and different $Z_{i,j}$ of a few impurities can be observed in the EAST by the fast-time response EUV spectrometer.[23] However, it is hard to give impurity concentrations of each charge state in current diagnostic system. Here, based on Ref. [22], average charge states $\langle Z_i \rangle_j$ are used to calculate the bombardment energy of the impurity ion in order to assess the sputtered W yield by multiple impurities for simplicity.

When the plasma hits the W target, W is mainly produced by physical sputtering process. Here the empirical formulas proposed by Yamamura is used to calculate the physical sputtering yield for the normal incidence of a projectile on a target[24]

$$Y(E_i) = 0.42 \frac{Q(Z_2)\alpha(M_2/M_1)}{U_s} \frac{S_n(E_i)}{1+\Gamma_f k_e \varepsilon^{0.3}} (1-\sqrt{E_{th}/E_i})^{s_{Z_2}}, \tag{8}$$

where Z_1 and Z_2 are the atomic numbers of incident and target atoms, $M_1 M_2$ are their mass numbers, respectively. Q_{Z_2} and s_{Z_2} are the parameters which depend only on the target material, the factors $\Gamma_f = \frac{w(z_2)}{1+(M_1/7)^3}$ and $\alpha(\frac{M_2}{M_1}) = 0.249(\frac{M_2}{M_1})^{0.56} + 0.0035(\frac{M_2}{M_1})^{1.5}$. The Lindhard electronic stopping coefficient

$$k_e = 0.079 \frac{(M_1+M_2)^{3/2}}{M_1^{3/2} M_2^{1/2}} \frac{Z_1^{2/3} Z_2^{1/2}}{(Z_1^{2/3}+Z_2^{2/3})^{3/4}},$$

U_s is the sublimation energy, E_{th} is the threshold energy, ε is the reduced energy

$$\varepsilon = \frac{0.03255 M_2}{Z_1 Z_2 (M_1+M_2)(Z_1^{2/3}+Z_1^{2/3})^{1/2}} E_i,$$

and the nuclear stopping cross section

$$S_n(E_i) = \frac{8.478 Z_1 Z_2}{(Z_1^{2/3}+Z_2^{2/3})^{1/2}} \frac{M_1}{M_1+M_2} s_n(\varepsilon)$$

with the reduced nuclear stopping power $s_n(\varepsilon)$.[24] For the W target, $Q_{Z_2} = 0.72$, $s_{Z_2} = 2.8$, $w(z_2) = 2.14$ and $U_s = 8.90$. Figure 1(a) shows the dependence of the W physical sputtering yield on the bombardment energy at normal incidence with D ions and some common impurity ions during EAST discharges.

For the angular dependence of the physical sputtering, the calculated yield values at a given incident energy are calculated by another Yamamura formula[25]

$$Y(E_i, \theta) = Y(E_i)(\cos\theta)^{-f} \exp\left[f(1-1/\cos\theta)\cos\theta_{opt}\right], \tag{9}$$

where f and θ_{opt} are the adjustable parameters which can be obtained by fitting the experimental data for the given target material, θ is the incident angle. Figure 1(b) plots the angular dependence of the W physical sputtering caused by some ions with bombardment energy $E_i = 1000$ eV. However, in the current EAST discharges, the magnetic field strength is not very strong ($B \sim 2$ T), and it is shown from the particle-in-cell simulation that the incident angle of W physical sputtering yield by impurity bombardment in the absence of the magnetic field can be approximately expressed as[18]

$$\cos\theta \approx \sqrt{E_{i,j}^{\perp}} / \sqrt{E_{i,j}}, \tag{10}$$

where $E_{i,j}^{\perp} = k_B T_{i,j} - Z_{i,j} e \Phi$ is the impurity average energy in the vertical divertor target direction. For the D ion with small mass, the incident angle depends on the magnetic field direction with respect to the divertor target and magnetic field strength. According to Ref. [15], $\theta = 64^\circ$ is used to calculate the D ions in this work.

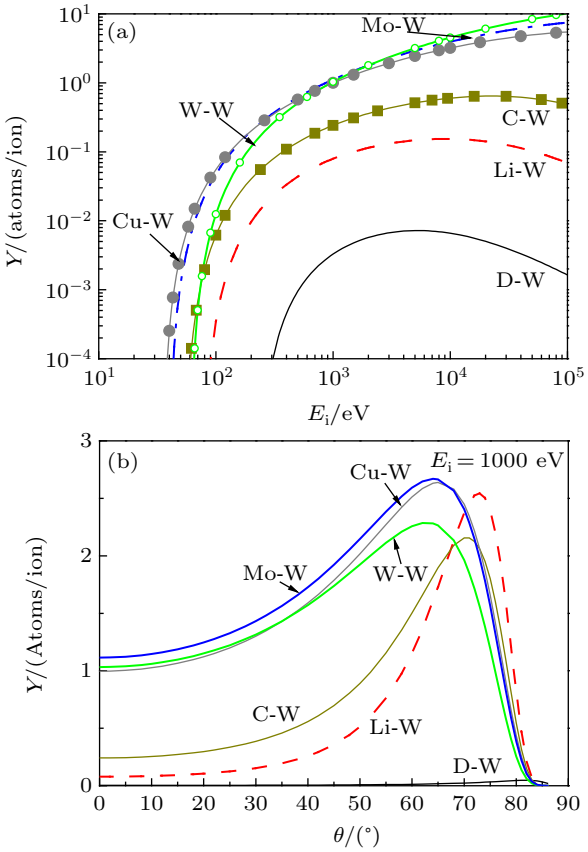


Fig. 1. (a) Energy dependence of the sputtered W yields for bombardment at normal incident with D, Li, C, Cu, Mo and self-sputter ions. (b) The W physical sputtering yield as a function of incident angle for bombardment energy $E_i = 1000$ eV due to D, Li, C, Cu, Mo and self-sputter ions.

3. Results

For the typical H-mode discharge with ELMs in the current EAST, $L_{\parallel} = 20$ m, $B \sim 2$ T and the angle between magnetic field lines and divertor target plate is 5°. In the divertor region, $n_{e,0}^0 = 10^{19}$ m^{-3} and $T_{e,0} = 10$ eV.

Firstly, we investigate how the sheath potential is changed by the ELM. Figure 2 shows the evolution of the plasma density at the sheath edge due to the ELM, particle fluxes at the target and the sheath potential during an ELM pulse. As the ELM propagates to the divertor target region, the hot plasma density and the corresponding hot particle fluxes increase and then decrease after peak. Once the hot plasma carried by the ELM hits the divertor target, a new balance of the ion and electron currents is needed to keep the zero current at the wall. Figure 2(b) shows the evolution of particle fluxes at the target in an ELM. The total ion flux including background and hot ion fluxes is mainly balanced by the hot electron flux during the ELM, and the ion flux is dominated by the background ion flux. In this process, the sheath potential has a large drop, as shown in Fig. 2(c), and the maximum sheath potential $-e_0\Phi^{\max}$ is far beyond $3k_BT_{e,0}$. If the sheath potential is normalized to the pedestal temperature, the maximum of the normalized sheath potential $-e_0\Phi^{\max}/k_BT_{ped} \approx 1.8$. The greater sheath potential can be found even after the peak of the ELM. At the end of the ELM pulse, the sheath potential resumes since the main balance of the particle flux is dominated by $\Gamma_{e,0} = \Gamma_{i,0}$. It is indicated from Fig. 2 that the large potential drop across the sheath is formed during ELMs by compared with inter-ELMs, and the sheath potential during ELMs is mainly determined by the hot electron flux carried by ELMs and background ion flux at the target.

Effect of the pedestal temperature on the evolution of the sheath potential is shown in Fig. 3(a). The drop of the sheath potential is larger in the whole ELM pulse process when the pedestal temperature is increased. This due to the fact that the sheath needs the larger potential drop to reduce the hot electron flux carried by ELMs at the divertor target since the total ion flux is mainly balanced by the hot electron flux, as demonstrated in Fig. 2(b). Figure 3(b) gives the variation of the maximum of the sheath potential with the pedestal plasma density and temperature in current EAST discharges based on the pedestal structure in type-I ELMy H-mode plasmas.[26] It is found that the maximum of sheath potential increases when the density and temperature are increased, and it can exceed 1 keV for the typical pedestal plasma parameters. From Fig. 3, it is shown that $-e_0\Phi^{\max}/k_BT_{ped} > 2$ with the high pedestal density and temperature in current EAST discharges. According to Eq. (7), the bombardment energy of hot D ions carried by ELMs on the divertor target $E_i/k_BT_{ped} \approx 5$, and the result is consistent with the prediction of the FSM shown in Ref. [8]. Moreover, the enhancement of the ion bombardment energy indicates that the W physical sputtering by the D ion impact is not negligible because the D ion has the higher bombardment energy compared to its threshold energy, and by the impurity ion impact increases, as shown in Fig. 1(a).

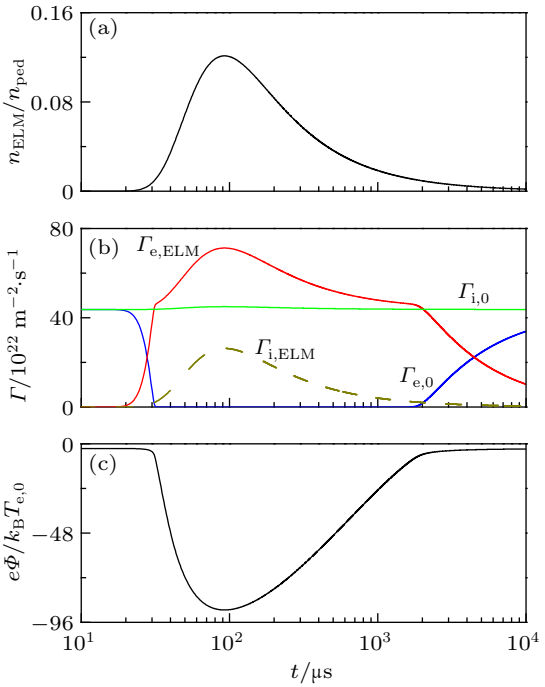


Fig. 2. The time evolution of the plasma density at the sheath edge due to ELMs (a), particle fluxes at the target (b), and the sheath potential (c) for $n_{ped} = 2 \times 10^{19}$ m^{-3} and $T_{ped} = 480$ eV.

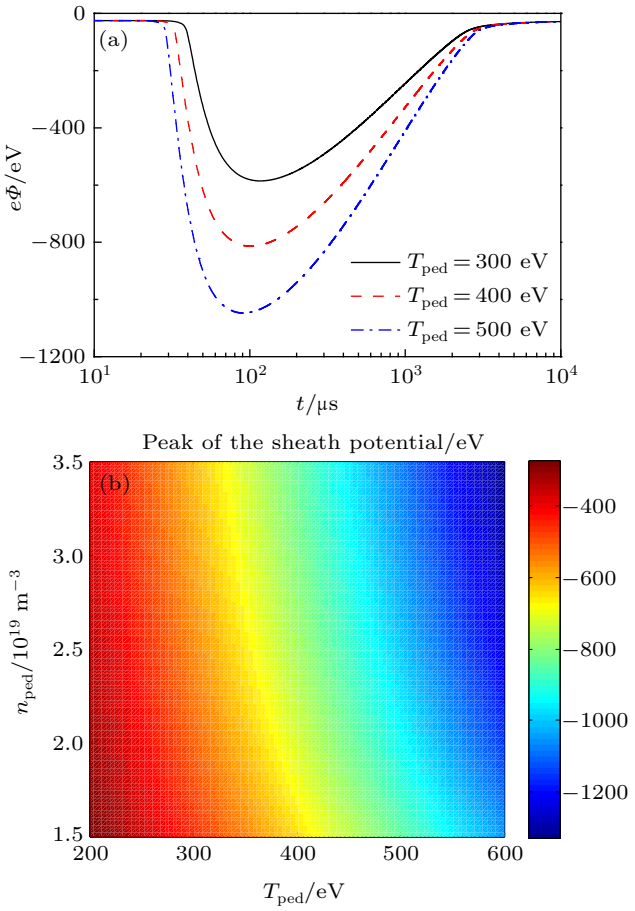


Fig. 3. The evolution of the sheath potential during ELMs for different temperatures in the pedestal region with $n_{ped} = 3 \times 10^{19}$ m^{-3} (a), and the maximum of the sheath potential as functions of the plasma density and temperature in the pedestal region (b).

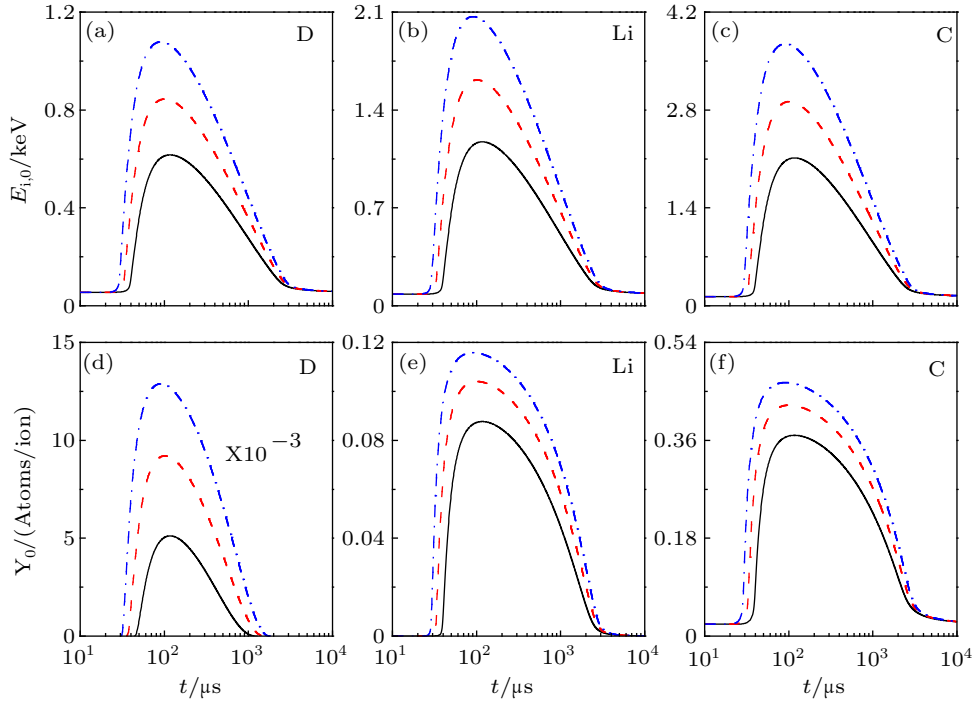


Fig. 4. During the ELM, the time evolution of impact energies of background ions (a) D, (b) Li, and (c) C; and W physical sputtering yield by corresponding ions of (d) D, (e) Li, and (f) C; for $n_{\rm ped} = 3 \times 10^{19}$ m^{-3} and different temperatures in the pedestal region. The black solid line is for $T_{\rm ped} = 300$ eV, the red dashed line is for $T_{\rm ped} = 400$ eV, and the blue dot-dashed line is for $T_{\rm ped} = 500$ eV.

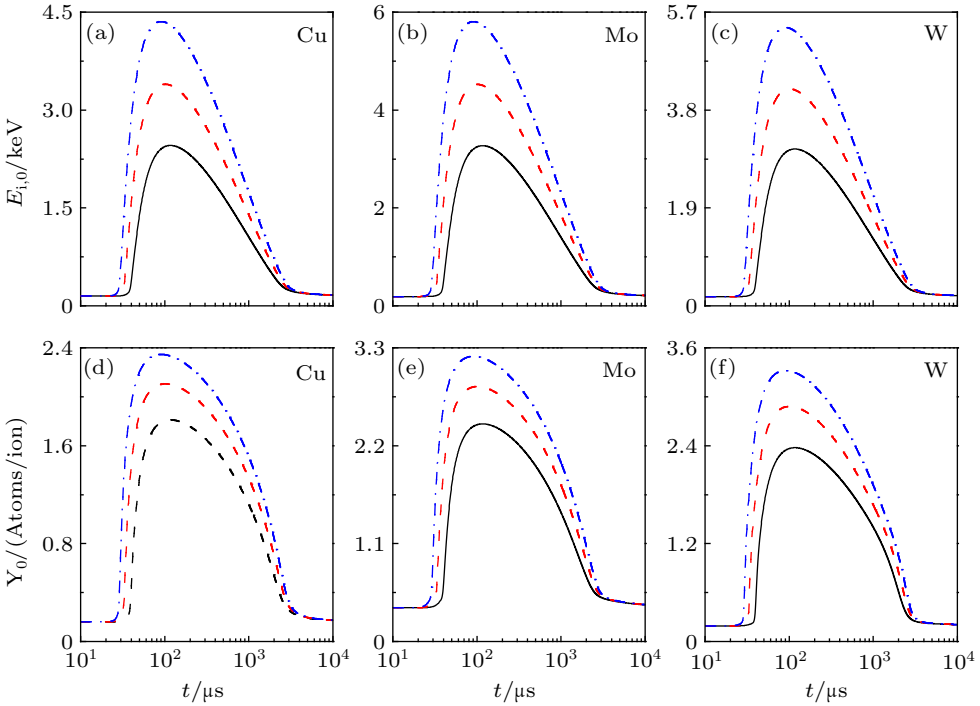


Fig. 5. During the ELM, the time evolution of impact energies of background ions (a) Cu (b) Mo and (c) W, and W physical sputtering yield by the corresponding ions (d) Cu (e) Mo and (f) W for $n_{\rm ped} = 3 \times 10^{19}$ m^{-3}. The black solid line is for $T_{\rm ped} = 300$ eV, the red dashed line is for $T_{\rm ped} = 400$ eV, and the blue dot-dashed line is for $T_{\rm ped} = 500$ eV.

The ion impact energy on the divertor target can be increased during ELMs as a result of the enhancement of the sheath potential drop. It is the decisive parameter for the physical sputtering to cause W production. In the EAST, besides the main ions of D, the impurity ions from the mixed wall materials and Li ions due to wall coating also impact on the divertor target and are the potential contributors causing the W production. To investigate the W production from upper divertor during ELM, we show the evolutions of the W physical sputtering yields caused by background D ions and common impurity ions including Li, C, Cu, Mo W, and the corresponding ion bombardment energies in Figs. 4 and 5. Before the arrival of hot plasma carried by the ELM at the divertor target, the sputtered W yield caused by D ions can be neglected be-

cause the impact energy is below the threshold energy, while the yield caused by C ions is about 0.02. With the assumption that the C concentration is a few percent in the EAST upper divertor region,[12,13] the sputtered W flux Γ_w from the divertor target is about $10^{-4}\Gamma_{i,0}$, which is consistent with the experimental results.[12] Although the heavy metal ions such as Cu, Mo and W can cause sputtered W yield to exceed 0.1, their concentration is usually 10^{-5}.[6,27] Our results also suggest that C impurity is the main impurity governing W source without the effect of ELMs, which is in agreement with the results shown in Ref. [12]. Following the evolution of the sheath potential shown in Fig. 3(a), the impact energies of the D ions and impurity ions increase rapidly and then decrease after peak during ELM. According to Eq. (7), the variation of the ion impact energies is mainly determined by the sheath potential during the ELM. With the enhancement of the sheath potential drop, the D ions become the contributor to the W source because the impact energy is higher than the threshold energy, although the maximum of the sputtering yield is less than 0.02 for $T_{ped} < 500$ eV. With increase in the pedestal temperature, the sputtered W yield from D ions on the divertor target increases rapidly, and the maximum increases about 3 times when pedestal temperature from 300 eV to 500 eV, as indicated in Fig. 4(d). With high averaged charge state, the impurity ions such as Li, C, Cu, Mo and W obtain more energy when across the sheath, and the resultant bombardment energies are larger than D ions. The maximum of the sputtered W yield from multiple impurity ions on the divertor target increases by one order of magnitude. However, the yield only increases about 50% for $T_{ped} = 500$ eV compared to the yield for $T_{ped} = 300$ eV.

To estimate the W production in a whole ELM pulse, we assume that the effect of the ELM on the divertor target from 30 μs to 3000 μs based on Fig. 2. The averaged sputtered W yield $\bar{Y}_0$ caused by background multiple ions are listed in Table 1. If the concentrations of multiple ions are the same as the inter-ELMs, i.e., C concentration is a few percent and heavy metal ions is 10^{-5}, the sputtered W flux caused by C impact can reach $10^{-3}\Gamma_{i,0}$ and it is the same order of magnitude caused by D ion impact. The sputtered W flux caused by heavy impurity ions is only about $10^{-5}\Gamma_{i,0}$. Therefore, in comparison to the inter-ELM W flux, the W flux caused by bombardment of multiple ions increases by one order of magnitude, and C and D ions are suggested as the two main contributors causing the W production for the current EAST discharges during ELMs. However, with increase in the pedestal temperature, the averaged sputtered W flux due to D ions increases rapidly, which indicates that D ions may become the potential main trigger of W source for the higher input power H-mode with ELM discharges when the concentration of C ions is controlled to be less than one percent. In fact, for the guard limiters of the 4.6 GHz lower hybrid wave heating system, the W material has been in place of the C material,[28] and the lower divertor target covering graphite tiles will be upgraded by using the W material in near future.[3]

Table 1. The averaged sputtered W yield caused by background multiple ions.

T_{ped}/eV	D	Li	C	Cu	Mo	W
Inter-ELMs		$< 10^{-5}$	0.0250	0.200	0.410	0.218
300	1.578×10^{-3}	0.0314	0.185	1.064	1.223	1.174
400	2.780×10^{-3}	0.0416	0.223	1.261	1.460	1.442
500	3.920×10^{-3}	0.0502	0.254	1.427	1.667	1.680

Table 2. Averaged sputtered W yield $\bar{Y}_{ELM}$ caused by hot multiple ions.

T_{ped}/eV	D	Li	C
300	1.097×10^{-2}	0.092	0.327
400	1.542×10^{-2}	0.109	0.373
500	1.896×10^{-2}	0.122	0.409

During ELMs, D ions and impurity ions in the pedestal region can be expelled by ELMs to the SOL and then impact on the divertor target. Due to the high ion energy at sheath edge, these hot ions have more higher impact energy than background ions. Since the concentration of the heavy metal impurity is very small in the core region, here we only investigate W sputtering yield from the D, Li and C ions carried by ELMs on the divertor target. Figure 6 shows the impact energies of the hot D ions, Li and C ions, and they cause W physical sputtering yield in an ELM pulse. By compared with the results shown in Figs. 4(d)–4(f), the sputtered W yields become larger than those caused by background ions, and the maximum of the sputtered W yield caused by D ions can exceed 0.01 while the yield caused by C ions does not increase notably.

From Table 2, the averaged sputtered W yield caused by hot D ions is about an order of magnitude higher than that caused by background D ions shown in Table 1. It is indicated that the sputtered W flux caused by hot D ions is larger than that caused by hot C ions if concentration of C ions is 1% in the pedestal region. However, according to Fig. 2(a), since $\Gamma_w = \bar{Y}_{ELM}\bar{n}_{e,ELM}C_{s,ELM}$ with the averaged $\bar{n}_{e,ELM} \approx 0.03 n_{ped}$ in an ELM pulse, the sputtered W flux caused by hot ions carried by ELM is at least one order of magnitude less than that caused by background ions. Therefore, the W production is mainly dominated by background ions instead of hot ions carried by ELMs.

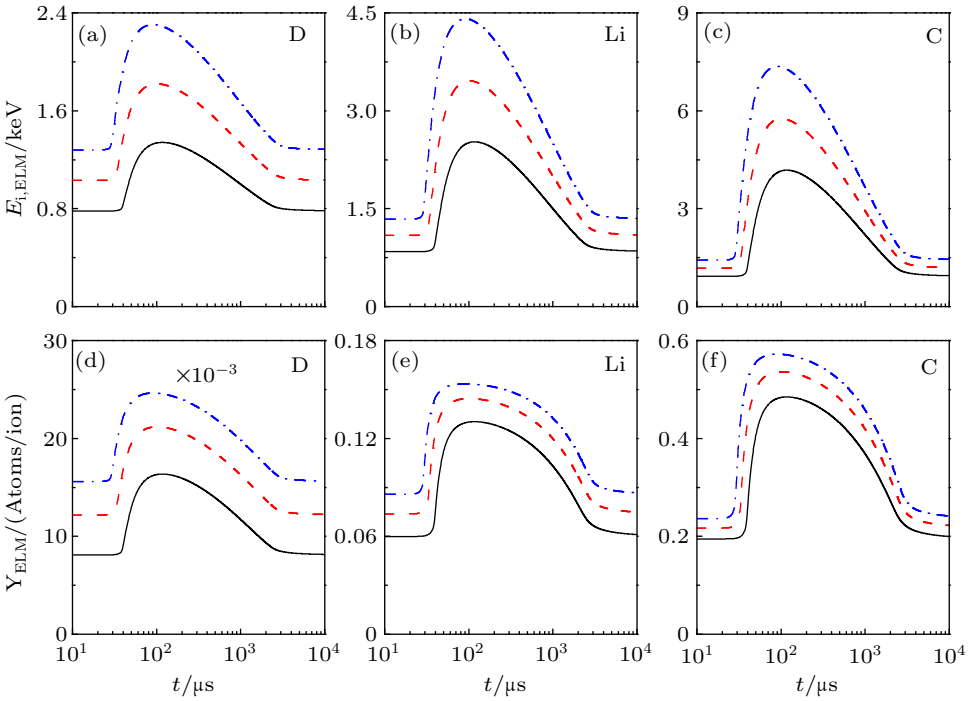


Fig. 6. During the ELM, the time evolution of impact energies of the ions (a) D, (b) Li, and (c) C carried by the ELM, and W physical sputtering yield by the corresponding ions (d) D, (e) Li, and (f) C for $n_{ped} = 3 \times 10^{19}$ m^{-3} at different temperatures in the pedestal region. The black solid line is for $T_{ped} = 300$ eV, the red dashed line is for $T_{ped} = 400$ eV, and the blue dot-dashed line is for $T_{ped} = 500$ eV.

Finally, we discuss the variation of the ion impact energy and the corresponding W sputtering yield with the pedestal temperature. In the JET, the experimental results have shown that the main ion impact energy depends linearly on the pedestal temperature.[11] In the current EAST, the sputtered W yield from C ions on the divertor target should not be ignored since C impurity is the main contributor for the W source. Here we investigate the dependence of maximum impact energy of the D ions and C ions on the pedestal temperature. For both background ions and hot ions carried by ELMs, it is shown in Fig. 7 that their maximum of the impact energy almost increases linearly because the maximum of sheath potential drop is close to linear increase with pedestal temperature, as shown in Fig. 3(b). The maximum of the sputtered W yield caused by D and C depends on the pedestal temperature is also shown in Fig. 7. For the high pedestal temperature and density, the background D ion impact energy can exceed 1 keV and the sputtered W yield is close to 2%. The hot D ion impact energy is above 1 keV when $T_{ped} > 300$ eV and the corresponding sputtered W yield exceeds 1%. The sputtered W yield from both the background and hot C ions on the divertor target is not more than 0.7 even for the case of $T_{ped} = 800$ eV. According to Fig. 1, the sputtered W yield caused by C ions is always less than 1. Therefore, for the high input power injection discharges in the EAST, the D ions during ELMs can become the main potential trigger of the W source due to the large sheath potential drop for high pedestal temperature if the impurity concentration is well controlled in near future.

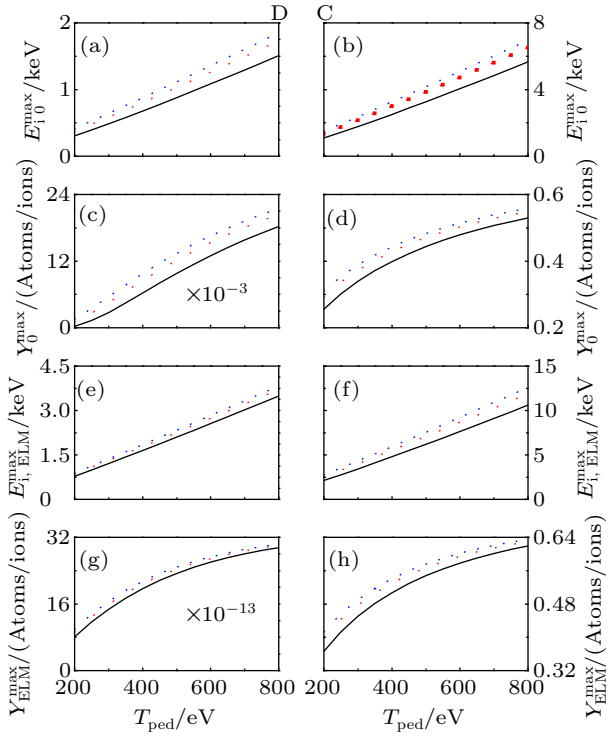


Fig. 7. Maximum of the D and C ion impact energy and the corresponding sputtered W yield as a function of the pedestal temperature for different densities in the pedestal region (a)–(d) due to the background ions and (e)–(h) due to the hot ions carried by ELMs. The black solid line is for $n_{ped} = 1.5 \times 10^{19}$ m^{-3}, the red dashed line is for $n_{ped} = 2.5 \times 10^{19}$ m^{-3}, and the blue dot-dashed line is for $n_{ped} = 3.5 \times 10^{19}$ m^{-3}.

4. Conclusions

During ELMs in EAST H-mode discharges, the transient enhanced energy deposition on the upper divertor target can cause the strong W physical sputtering. To estimate the sput-

tered W atoms from the divertor target, the evolution of the sheath potential in an ELM pulse is investigated with the 'free-streaming' kinetic model which describes ELMs. The large potential drop across the sheath can be formed in front of the divertor target during ELMs by compared with inter-ELMs. It is found that the maximum of sheath potential drop depends on the arrival of the pedestal bulk plasma temperature and density, and it can exceed one thousand of eV in the current EAST operation.

For the current operation in the EAST, with the enhancement of the sheath potential drop during ELMs, the background D ions can obtain the impact energy beyond threshold energy and then become one of the contributors causing the W production. For the background impurity ions such as Li, C, Cu, Mo and W, the maximum of sputtered W yield caused by their bombardment increases by one order of magnitude compared to the inter-ELMs. The results also show that the averaged sputtered W flux caused by D ions during ELMs is comparable to that caused by C ions since the C ion concentration is more than one percent in the current EAST upper dvertor region. It is suggested that C and D ions are the main ions governing the sputtered W flux from the upper divertor target during the ELMs burst. However, with increase in the heating power in near future, the W physical sputtering yield from background D ions on the divertor target surface increases rapidly due to the increase in the pedestal temperature. The averaged sputtered W flux caused by D ions may be larger than that caused by the C ions if concentration of C ions is less than one percent, and then the D ion becomes the potential main trigger of the W source for high heating power discharges in near future. Finally, it should be noted that in the present work, we focus on the W production while neglect the energy reflections and W re-deposition processes. In the further works, the effect of the magnetized sheath on the energy reflection and W re-deposition will be included.

References

[1] Krieger K, Maier H, Neu R and ASDEX Upgrade Team 1999 *J. Nucl. Mater.* **266–269** 207

[2] Matthews G F, Beurskens M, Brezinsek S, Groth M, Joffrin E, Loving A, Kear M, Mayoral M L, Neu R, Prior P, Riccardo V, Rimini F, Rubel M, Sips G, Villedieu E, de Vries P, Watkins M L and EFDA-JET contributors 2011 *Phys. Scr.* **T145** 014001

[3] Yao D, Luo G, Du S, Cao L, Zhou Z, Xu T, Ji X, Liu C, Liang C, Li Q, Wang W, Zhao S, Xu Y, Li L, Wang Z, Xiao X, Qi M, Wang S and Li J 2015 *Fusion Eng.* **98–99** 1692

[4] Wan Y, Li J, Liu Y, Wang X, Chan V, Chen C, Duan X, Fu P, Gao X, Feng K, Liu S, Song Y, Weng P, Wan B, Wan F, Wang H, Wu S, Ye M, Yang Q, Zheng G, Zhuang G, Li Q and CFETR team 2017 *Nucl. Fusion* **57** 102009

[5] Wan B N, Liang Y F, Gong X Z, Li J G, Xiang N, Xu G S, Sun Y W, Wang L, Qian J P, Liu H Q, Zhang X D, Hu L Q, Hu J S, Liu F K, Hu C D, Zhao Y P, Zeng L, Wang M, Xu H D, Luo G N, Garofalo A M, Ekedahl A, Zhang L, Zhang X J, Huang J, Ding B J, Zang Q, Li M H, Ding F, Ding S Y, Lyu B, Yu Y W, Zhang T, Zhang Y, Li G Q, Xia T Y, EAST team and Collaborators 2017 *Nucl. Fusion* **57** 102019

[6] Garofalo A M, Gong X Z, Qian J, Chen J, Li G, Li K, Li M H, Zhai X, Bonoli P, Brower D, Cao L, Cui L, Ding S, Ding W X, Guo W, Holcomb C, Huang J, Hyatt A, Lanctot M, Lao L L, Liu H, Lyu B, McClenaghan J, Peysson Y, Ren Q, Shiraiwa S, Solomon W, Zang Q and Wan B 2017 *Nucl. Fusion* **57** 076037

[7] Philipps V 2011 *J. Nucl. Mater.* **415** S2

[8] Moulton D, Ghendrih Ph, Fundamenski W, Manfredi G and Tskhakaya D 2013 *Plasma Phys. Control. Fusion* **55** 085003

[9] Bergmann A 2002 *Nucl. Fusion* **42** 1162

[10] Dai S and Wang D 2018 *Nucl. Fusion* **58** 014006

[11] Guillemaut G, Jardin A, Horacek J, Borodkina I, Autricque A, Arnoux G, Boom J, Brezinsek S, Coenen J W, Luna E De La, Devaux S, Eich T, Harting D, Kirschner A, Lipschultz B, Matthews G F, Meigs A, Moulton D, O'Mullane M, Stamp M and JET contributors 2016 *Phys. Scr.* **T167** 014005

[12] Mao H, Ding F, Luo G, Hu Z, Chen X, Xu F, Hu J, Zuo G, Sun Z, Yu Y, Wu J, Wang L, Duan Y, Xu J, Chen J, Yang Z, Ding R, Xie H and EAST team 2017 *Nucl. Mater. Energy* **12** 447

[13] Xie H, Ding R, Kirschner A, Chen J L, Ding F, Mao H M, Feng W, Borodin D and Wang L 2017 *Phys. Plasmas* **24** 092512

[14] Wang F, Zha X J, Duan Y M, S T Mao S T, Wang L, Zhong F C, Liang L, Li L, Lu H W, Hu L Q, Chen Y P and Yang Z D 2018 *Plasma Phys. Control. Fusion* **60** 125005

[15] Dai S, Wang L, Kirschner A and Wang D 2015 *Nucl. Fusion* **55** 043003

[16] Havlickova E, Fundamenski W, Tskhakaya D, Manfredi G and Moulton D 2012 *Plasma Phys. Control. Fusion* **54** 045002

[17] Manfredi G, Hirstoaga S and Devaux S 2011 *Plasma Phys. Control. Fusion* **53** 015012

[18] Sun Z, Sang C, Hu W and Wang D 2014 *Acta Phys. Sin.* **63** 145204 (in Chinese)

[19] Franklin R N 2003 *J. Phys. D: Appl. Phys.* **36** 1806

[20] Lin B, Xiang N, Ou J and Zhao X 2017 *Chin. Phys. Lett.* **34** 015203

[21] Riemann K U 1995 *IEEE Transaction Plasma Science* **23** 709

[22] Chung H K, see https://www-amdis.iaea.org/FLYCHK/ for NLTE kinetics modeling code

[23] Zhang L, Morita S, Xu Z, Wu Z, Zhang P, Wu C, Gao W, Ohishi T, Goto M, Shen J, Chen Y, Liu X, Wang Y, Dong C, Zhang H, Huang X, Gong X, Hu L, Chen J, Zhang X, Wan B and Li J 2015 *Rev. Sci. Instrum.* **86** 123509

[24] Yamamura Y 1996 *At. Data Nucl. Data Tables* **62** 149

[25] Yamamura Y, Itikawa Y and Itoh N 1983 *Angular dependence of sputtering yields of monoatomic solids* Institute of Plasma Physics, Nagoya, Japan Report number IPPJ-AM-26

[26] Han X, Zang Q, Xiao S, Wang T, Hu A, Tian B, Li D, Zhou H, Zhao J, Hsieh C, Li M, Yan N, Gong X, Hu L, Xu G, Gao X and EAST team 2017 *Plasma Phys. Control. Fusion* **59** 045007

[27] Dong L, Duan Y, Chen K, Yang X, Zhang L, Xu F, Chen J, Mao S, Wu Z and Hu L 2018 *Plasma Sci. Technol.* **20** 065102

[28] Liu C, Zhang L, Cao L, Li L, Han L, Wang Z, Xu H, Liu Y, Liu L, Yao D, Gong X and Song Y 2017 *Fusion Eng.* **125** 93